

# Current helicity pattern of large-scale magnetic field on the photosphere

WANG ChuanYu<sup>†</sup> & ZHANG Mei

Key Laboratory of Solar Activity, National Astronomical Observatories, Chinese Academy of Sciences, Beijing 100012, China

**Following Pevtsov and Latushko, we study the current helicity pattern of the large-scale magnetic field on the photosphere. We use the same technique as theirs to derive the vector magnetic field ( $B_r, B_\theta, B_\phi$ ) from full-disk longitudinal magnetograms based on the assumption that large-scale magnetic fields evolve rather slowly and the variations of the longitudinal magnetic fields within certain time duration are caused by the changing position angles only. Different from their study, we have calculated the current helicity maps directly from the derived vector magnetograms, rather than from obtaining the latitudinal variation of  $h_c$  by ignoring the role of  $B_\theta$  component and averaging  $B_r$  and  $B_\phi$  over all solar longitudes. This approach significantly strengthens the evidence of the hemispheric rule presented in the reconstructed vector magnetic field. Our study shows that the established hemispheric sign rule, that is, positive helicity sign in the southern hemisphere and negative helicity sign in the northern hemisphere, is applicable everywhere in the global magnetic field, namely, also evident in weak fields outside active regions, and that the obtained sign pattern is independent of the longitudinal magnetograms and the parameters that we have used.**

Sun: Activity, magnetic fields, current helicity

Magnetic helicity was first introduced as a mathematical description of the topological invariance of the complexity of a magnetic field, such as the degree of linkage and/or twistedness in the field<sup>[1,2]</sup>. Its physical meaning soon became more evident and prominent after Berger<sup>[3]</sup> found that its total amount is approximately conserved in the Sun during most coronal processes, even during fast magnetic reconnection. This important conservation law has been successfully applied to various solar phenomena studies. For example, magnetic helicity

and its conservation are assumed to play an important role in CME dynamics<sup>[4,5]</sup>, where the accumulation of total magnetic helicity in the respective northern and southern hemispheres makes the CME-type eruptions natural and unavoidable products of coronal evolution<sup>[6–8]</sup>.

By current observational feasibility, only vector magnetic fields on the photosphere can be measured relatively precisely. That is to say, we cannot yet directly measure magnetic helicity. In practice, only the vertical component of current helicity

Received July, 29, 2009; accepted August 25, 2009

doi: 10.1007/s11433-009-0251-6

<sup>†</sup>Corresponding author (email: wangchuanyu@bao.ac.cn)

Supported by the National Natural Science Foundation of China (Grant Nos. 40636031 and 10778723), the Important Directional Projects of Chinese Academy of Sciences (Grant No. KLCX2-YW-T04), and the National Basic Research Program of China (Grant No. 2006CB806301)

**Citation:** Wang C Y, Zhang M. Current helicity pattern of large-scale magnetic field on the photosphere. *Sci China Ser G*, 2009, 52(11): 1713-1717, doi: 10.1007/s11433-009-0251-6

density of one layer can be measured by the vector magnetograms measured on the photosphere. Previous statistical studies<sup>[9,10]</sup> shows that magnetic fields possess a positive current helicity sign in the southern hemisphere and a negative current helicity sign in the northern hemisphere. These results are obtained from the vector magnetic field measurements in active regions only because of the limited sensitivity of the instruments.

Pevtsov & Latushko<sup>[11]</sup> were the first to study the current helicity of the global Sun outside active regions, by applying a reconstruction technique to full-disk longitudinal magnetograms. They found that the usual hemispheric rule is applicable in regions above 40° of solar latitude whereas the rule is surprisingly not obvious for regions within 40° of solar latitude where there are active regions. This seems to be consistent with the report<sup>[12]</sup> that strong and weak magnetic fields display opposite helicity signs, where the weak fields, not strong fields, follow the established hemispheric helicity rule.

In this paper we study the current helicity pattern of the global Sun on the photosphere by following Pevtsov and Latushko. Since current full-disk vector magnetograms<sup>[13]</sup> are still very noisy in the quiet-Sun regions, the approach in Pevtsov and Latushko is taken to reconstruct the vector magnetic field of the global Sun from longitudinal magnetograms. Different from their study, with a different method we calculate the current helicity profile with the latitude.

## 1 Reconstruction technique

Consider the spherical coordinate system  $(r, \theta, \phi)$  where  $r, \theta, \phi$  are radius, polar angle (colatitude) and longitude respectively, and the magnetic field is represented by its radial ( $B_r$ ), meridional ( $B_\theta$ ) and toroidal ( $B_\phi$ ) components. On the photosphere where  $r = 1$ , the observed longitudinal magnetic field ( $B_{\text{long}}$ ) can be described by

$$B_{\text{long}}(\theta, \phi) = \mathcal{R}(\theta, \phi) \cos \phi \cos B_0 + \mathcal{P}(\theta, \phi) \sin B_0 + \mathcal{T}(\theta, \phi) \sin \phi \cos B_0, \quad (1)$$

where  $B_0$  is the latitude of the solar disk center,

and

$$\begin{aligned} \mathcal{R}(\theta, \phi) &= B_r(\theta, \phi) \sin \theta + B_\theta(\theta, \phi) \cos \theta, \\ \mathcal{P}(\theta, \phi) &= B_r(\theta, \phi) \cos \theta - B_\theta(\theta, \phi) \sin \theta, \\ \mathcal{T}(\theta, \phi) &= -B_\phi(\theta, \phi). \end{aligned} \quad (2)$$

Now, we assume that the magnetic field evolves rather slowly and we interpret the variation of the observed  $B_{\text{long}}$  (during a period of time) as the result of changing position angles only. Then, using a set of observed  $B_{\text{long}}$  maps and applying the above equations we can reconstruct the synoptic maps of  $B_r$ ,  $B_\theta$  and  $B_\phi$ . For example, we take the  $B_{\text{long}}$  map of a day, say, September 20, 1996 and get the  $B_{\text{long}}$  value of a point in its central meridional zone. Then we choose a characteristic time period  $\Delta t$ , say, 5 d, as in Pevtsov & Latushko, and calculate where this point was or would be 5 d before or after. Then we try to find the  $B_{\text{long}}$  values from the maps taken 5 d before or after. Now we have three  $B_{\text{long}}$  values of this point but at different position angles. Applying eqs. (1) and (2) to these three  $B_{\text{long}}$  values we can then get the  $B_r$ ,  $B_\theta$  and  $B_\phi$  values of this point. Similarly we can get  $B_r$ ,

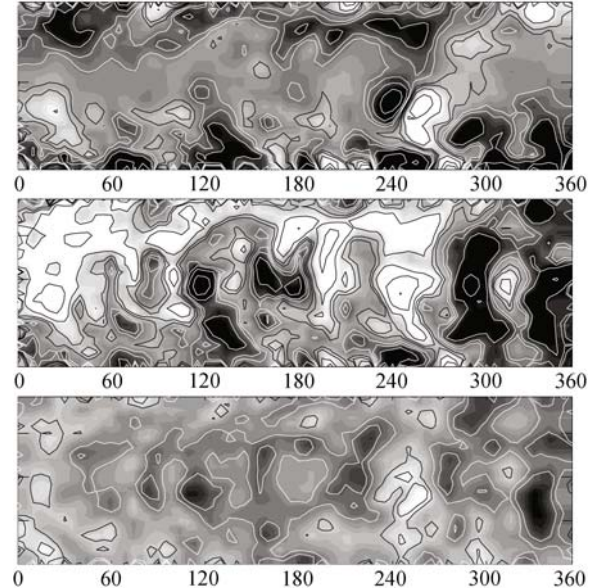


**Figure 1** Constructed snapshot heliographic maps of  $B_r$ ,  $B_\theta$ ,  $B_\phi$ , from top to bottom panels respectively, of one solar rotation. The white background represents positive values of  $B_r$  (pointing up),  $B_\theta$  (pointing to the north) and  $B_\phi$  (pointing to the left) respectively. Contours correspond to  $\pm 2, 4, 8, 16, 32, 64G$  for  $B_r$  and  $B_\theta$ , and  $\pm 0.5, 1, 2G$  for  $B_\phi$ .

$B_\theta$  and  $B_\phi$  values of different points with different Carrington longitude and latitude to draw synoptic maps of  $B_r$ ,  $B_\theta$  and  $B_\phi$ .

The key assumption of this construction is that the magnetic field evolves rather slowly and the variation of the observed  $B_{\text{long}}$  during a period of time is the result of changing position angles only. As also discussed in Pevtsov & Latushko, we know that the magnetic fields on small spatial scales evolve rather significantly over short time scales such as minutes and hours. But the point is that the large-scale magnetic field exhibits structures that persist for several months. We are interested in this large-scale structure, so a proper choice of the characteristic time  $\Delta t$  (during which the large-scale field does not change much) and the sliding window  $\Delta S$  (reducing the spatial resolution to keep the large-scale structure only) will render the construction reasonable. Pevtsov & Latushko found  $\Delta t = 5$  d and  $\Delta S = 184''$  the best choice for the five-minutes-averaged full-disk MDI magnetograms they used. Since we are also using the same type of MDI data, we will first follow their choice. Later on, we will use different numbers of  $\Delta t$  and  $\Delta S$  to check whether our results depend on the choice of these numbers.

In the construction we also need to know the profile of differential rotation. Applying the cross-correlation method<sup>[14]</sup> to the original high-resolution MDI magnetograms, Pevtsov & Latushko computed the mean rotation profile and found the polynomial approximation of this profile as

$$W(\theta) = (13.51 \pm 0.03) - (1.72 \pm 0.22) \cos^2 \theta - (2.31 \pm 0.30) \cos^4 \theta, \quad (3)$$

where  $W$  is the angular velocity in units of degrees per day and  $\theta$  is the colatitude. Again, we will use the same profile as they found because we are using the same family of data as theirs.

Note that in using differential rotation rate as presented in eq. (3), we have constructed the “snapshot heliographic maps” described in Ulrich & Boyden<sup>[14]</sup>, rather than the traditional Carrington synoptic maps. The traditional Carrington synoptic maps are constructed by a fixed rotation rate, that is, the Carrington rotation rate. However, due

to the differential rotation on the solar surface, different parts on such a synoptic map are actually observed at different times. This is a simulation of Ulrich & Boyden<sup>[14]</sup> which uses the differential rotation rate instead of a fixed rotation rate to construct synoptic maps. The maps are named “snapshot heliographic maps”. Here we have also used snapshot heliographic maps, because in order to study the spatial variation of vector magnetic field (namely, current helicity) on the solar photosphere we need to know the vector magnetic field obtained at a fixed time so that a study of the spatial variation based on them becomes reasonable.

Figure 1 presents the snapshot heliographic maps of  $B_r, B_\theta, B_\phi$  of one solar rotation, constructed in this way. This synoptic map covers about the same period as that of Carrington Rotation 1914. But since we have used differential rotation rates (eq. (3)) for different latitudes, the MDI data we have used are actually of more than one month, from September 14, 1996 to October 31, 1996. The constructed synoptic map contains a grid that spans from  $-60^\circ$  to  $60^\circ$  in latitude and  $0^\circ$  to  $360^\circ$  in longitude with  $5^\circ$  steps in each coordinate.

## 2 Analysis and results

With the vector magnetic field obtained as that in Figure 1, we can compute the vertical component of current helicity density  $h_c$ . In the spherical coordinate system, we have

$$\begin{aligned} h_c(\phi, \theta) &= B_r(\nabla \times B)_r \\ &= \frac{1}{\sin \theta} \left\{ \frac{\partial}{\partial \theta} [\sin \theta B_\phi(\phi, \theta)] \right. \\ &\quad \left. - \frac{\partial B_\theta(\phi, \theta)}{\partial \phi} \right\} B_r(\phi, \theta). \end{aligned} \quad (4)$$

This gives the distribution of  $h_c$  as presented in Figure 2. From Figure 2, we see that  $h_c$  is mostly positive in the southern hemisphere and mostly negative in the northern hemisphere.

It is interesting to see that in Figure 2 the active region in the southern hemisphere shows a bulk area of negative  $h_c$  values, which are opposite to those of the surrounding regions. This seems consistent with the result of Zhang<sup>[12]</sup> where strong

and weak fields are found to have opposite helicity signs.



**Figure 2** The current helicity density  $h_c$  map. The white background represents positive values of  $h_c$ . Contours correspond to  $h_c = \pm 0.1, 0.2, 0.4, 0.8 \times 10^{-5} \text{ G}^2 \cdot \text{m}^{-1}$ .

To give a better representation of the hemispheric rule, we plot in Figure 3 the profile of the latitudinal distribution of averaged  $h_c$ . This profile is obtained by averaging the above  $h_c$  map over all longitudes of the same latitude. Figure 3 shows clearly the hemispheric rule, that is, positive helicity sign in the southern hemisphere and negative helicity sign in the northern hemisphere, for all latitudes, including the latitudes below  $40^\circ$ .

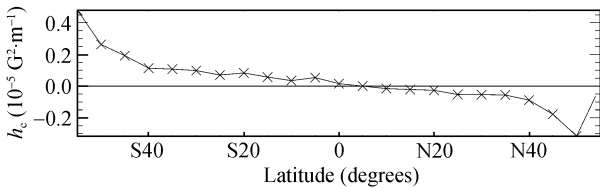


**Figure 3** The profile of averaged  $h_c$  with the latitude.

Note that our approach here is different from that of Pevtsov & Latushko where they have ignored the second term in eq. (4) and used a longitudinally-averaged  $B_r$  and  $B_\phi$  to replace point-by-point  $B_r$  and  $B_\phi$  in the first term of eq. (4). We have tried to use their approach which fails to produce a profile as good as that in Figure 3. Figure 4 is our profile acquired through their approach. We estimate two possible reasons for a better and clearer profile. First is some probable very useful information of  $h_c$  contained in the  $B_\theta$  magnetogram that Pevtsov & Latushko ignored. Note that Figure 1 shows typically larger  $B_\theta$  than  $B_\phi$  and a strong variation in  $\phi$ -direction. This indicates that the second term may actually be the largest term in eq. (4). Second, our method gives each point on the synoptic map an equal weight whereas theirs

are more heavily influenced by strong fields because they averaged the  $B_r$  and  $B_\phi$  before calculating  $h_c$ . Particularly, the difference may become more evident if the strong and weak fields show opposite helicity signs as reported in Zhang<sup>[12]</sup> and indicated in Figure 2.

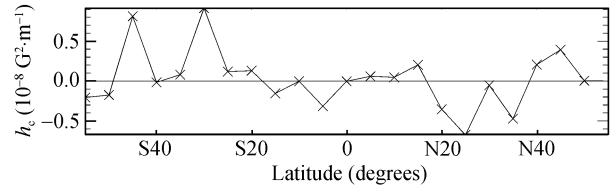


**Figure 4** The profile of averaged  $h_c$  with the latitude, by using Pevtsov & Latushko's approach.

Our next step is to check whether our results depend on the magnetograms used and parameters chosen. Figure 5 shows similar profiles of  $h_c$  as that in Figure 3, but these profiles are obtained from the synoptic maps that are constructed by using different magnetograms of each day. We know each day MDI has 15 full-disk magnetograms, that is, a 5-min full-disk magnetogram in every 96 min. To construct the synoptic maps in Figure 1, we have used the first magnetogram of each day. Now we have used other magnetograms of each day and constructed 15 different synoptic maps of vector magnetic field and hence get 15 different  $h_c$  profiles as shown in Figure 5. Here we have kept other parameters the same, that is,  $\Delta t = 5 \text{ d}$  and  $\Delta S = 184''$ . These profiles are found very similar to each other. They show the same hemispheric rule, independent of the magnetograms we have used.

When we change the  $\Delta t$  and  $\Delta S$ , we get similar profiles. This means our result is also independent

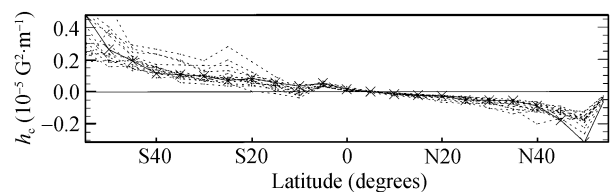


**Figure 5** Same as Figure 3, but here the solid line shows the profile using the first magnetograms of each day as that in Figure 3, and the dotted lines show the profiles using other 14 magnetograms of each day.

of the parameters we chose. Figure 6 shows the profiles created by using different  $\Delta t$  values and Figure 7 shows the profiles created with different  $\Delta S$  values.

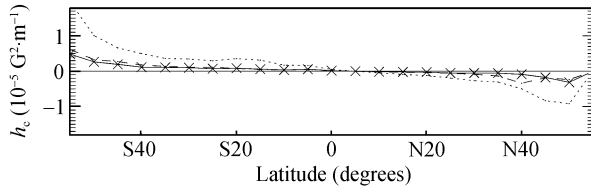


**Figure 6** Same as Figure 3, but here the solid line shows the profile using  $\Delta t = 5$  d, and the dotted and dashed lines show the profiles using  $\Delta t = 3$  and 4 d respectively.

### 3 Conclusion

We conclude that the large-scale magnetic fields show a clear and consistent current helicity pat-

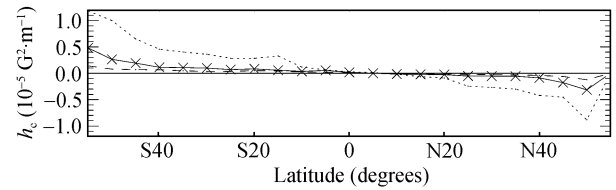


**Figure 7** Same as Figure 3, but here the solid line shows the profile using  $\Delta S = 184''$ , and the dotted and dashed lines show the profiles using  $\Delta S = 90''$  and  $224''$  respectively.

tern that follows the established hemispheric rule, that is, positive helicity sign in the southern hemisphere and negative helicity sign in the northern hemisphere. This hemispheric sign pattern is found everywhere in the global magnetic field, including weak fields outside the active regions, independent of the longitudinal magnetograms and the parameters we have used.

- 1 Moffatt H K. Magnetostatic equilibria and analogous Euler flows of arbitrarily complex topology. I - Fundamentals. *J Fluid Mech*, 1985, 159: 359–378
- 2 Berger M A, Field G B. The topological properties of magnetic helicity. *J Fluid Mech*, 1984, 147: 133–148
- 3 Berger M A. Rigorous new limits on magnetic helicity dissipation in the solar corona. *Geophys Astrophys Fluid Dyn*, 1984, 30: 79–104
- 4 Low B C. Coronal mass ejections, magnetic flux ropes, and solar magnetism. *J Geophys Res*, 2001, 106: 25141–25164
- 5 Démoulin P, Mandrini C H, van Driel-Gesztelyi L. What is the source of the magnetic helicity shed by CMEs? The long-term helicity budget of AR 7978. *Astron Astrophys*, 2002, 382: 650–665
- 6 Zhang M, Low B C. The hydromagnetic nature of solar coronal mass ejections. *Ann Rev Astron Astrophys*, 2005, 43: 103–137
- 7 Zhang M, Flyer N, Low B C. Magnetic field confinement in the corona: The role of magnetic helicity accumulation. *Astrophys J*, 2006, 644(1): 575–586
- 8 Zhang M, Flyer N. The dependence of the helicity bound of force-free magnetic fields on the boundary conditions. *Astrophys J*, 2008, 683(2): 1160–1167
- 9 Pevtsov A A, Canfield R C, Metcalf T R. Patterns of helicity in solar active regions. *Astrophys J*, 1994, 425(2): L117–L119
- 10 Bao S D, Zhang H Q. Patterns of current helicity for the twenty-second solar cycle. *Astrophys J Lett*, 1998, 496: L43
- 11 Pevtsov A A, Latushko S M. Current helicity of the large-scale photospheric magnetic field. *Astrophys J*, 2000, 528(2): 999–1003
- 12 Zhang M. Helicity observations of weak and strong fields. *Astrophys J*, 2006, 646(1): L85–L88
- 13 Zhang H Q, Wang D G, Deng Y Y. Solar magnetism and the activity telescope at HSOS. *Chin J Astron Astrophys*, 2007, 7(2): 281–288
- 14 Ulrich R K, Boyden J E. Carrington coordinates and solar maps. *Sol Phys*, 2006, 235(1-2): 17–29